Computers and Mathematics with Applications 65 (2013) 864–881

Contents lists available at SciVerse ScienceDirect

Computers and Mathematics with Applications

journal homepage: www.elsevier.com/locate/camwa

A lattice Boltzmann method for immiscible two-phase Stokes flow with a local collision operator

Jonas Tölke *, Giuseppe De Prisco, Yaoming Mu

Ingrain Inc., 3733 Westheimer Rd., Houston, TX 77027, USA

ARTICLE INFO

Keywords:
Lattice Boltzmann
Immiscible two-phase flow

ABSTRACT

We propose a lattice Boltzmann model for immiscible two-phase Stokes flow with a local collision operator. The model is based on two different lattice Boltzmann automata, one for the flow field and one for an indicator function for the two different phases. The model is described in detail and verified by the following test-cases: a static bubble for the surface tension, a closed capillary tube for the contact angle and two phase flow in a concentric annulus for the viscosity ratio. In the appendix an asymptotic analysis for the derivation of the two-phase Stokes equation is given.

1. Introduction

In the past two decades the lattice Boltzmann method (LBM) has matured to an alternative and efficient numerical scheme for the simulation of fluid flows and transport problems [1–4]. Unlike conventional numerical schemes based on discretizations of macroscopic continuum equations, the lattice Boltzmann method is based on microscopic models and mesoscopic kinetic equations. The fundamental idea of the LBM is to construct simplified kinetic models that incorporate the essential physics of microscopic or mesoscopic processes in a way that the macroscopic averaged properties obey the desired macroscopic equations.

The basis of the LBM is a simplified Boltzmann equation, where particle distribution functions (subsequently also called populations) propagate and collide on a regular lattice. In the collision the populations are over/under-relaxed towards an equilibrium described by a Maxwell–Boltzmann distribution. Even though the LBM is based on a particle picture, its principal focus is the averaged macroscopic behavior. The scheme is particularly successful in problems where transport problems are described by an advective and a diffusive operator. Examples are transport phenomena described by mass conservation like the (nonlinear) advection–diffusion equation and phenomena described by mass and momentum conservation like the (Navier–)Stokes equations. Especially applications involving interfacial dynamics, complex and/or changing boundaries and complicated constitutive relationships which can be gained from a microscopic picture are suitable for the LBM.

For two phase flow in porous media on the microscale especially in a tight pore space it is possible to neglect the inertia forces and the gravity. The system is then described by the Stokes equation and the dimensionless parameters which describe the dynamics of the system are the ratio of the dynamic viscosities and the capillary number:

$$M = \mu_1/\mu_2, \qquad Ca = \frac{k\nabla p}{\Phi\,\sigma}, \tag{1}$$

where μ_1 and μ_2 are the dynamic viscosities of the two phases, k is the absolute permeability, ∇p the pressure gradient, Φ the porosity and σ the interfacial tension. Also the contact angle has to be matched. Since we do not consider inertia forces nor gravity in this model, we do not use different densities for the two phases in the LB model. The dimensionless parameters M and Ca are matched through the viscosities, surface tension, velocities or the pressure gradient.

* Corresponding author. Tel.: +1 713 993 9795; fax: +1 713 993 9918.
E-mail address: toelke@ingrainrocks.com (J. Tölke).

0898-1221/$ – see front matter
doi:10.1016/j.camwa.2012.05.018

2. The LB method for three-dimensional two-phase Stokes-flow in porous media

The LBM is especially suitable for the direct numerical simulation of multi-component and immiscible multiphase fluid flows. Since LBM models belong to the class of diffuse-interface methods they do not track interfaces and sharp interfaces are maintained through different mechanisms. There are three standard LB-models for the simulation of immiscible two-phase systems: the first lattice gas model for immiscible binary fluids was proposed by Rothman and Keller in [5] and is labeled as Rothman–Keller (RK) model. The equivalent LBM was developed by Gunstensen and Rothman [6]. Grunau et al. [7] modified the model for binary fluids with different density and viscosity ratios on a triangular lattice in two dimensions. Shan and Chen [8] proposed a LBM model with mean-field interactions for multiphase and multi-component fluid flows (SC model). Swift et al. [9] developed a LBM model for multiphase and multi-component fluid flows using the free-energy approach (FE model). Ginzburg and Adler [10,11] has proposed and analyzed RK models with different viscosities in detail. In different publications [12–14] the algorithm to separate the two phases has been improved and also has been analyzed in depth in [15]. In [16] a volume-preserving sharpening approach for the propagation of sharp phase boundaries in multiphase lattice Boltzmann simulations is presented. In this work the reasons for lattice pinning and different effects for immiscible LB schemes are explained in detail. In the work of He et al. [17] two different LB automata are introduced, one for the flow field and one for an index function to track interfaces between different phases. Kim and Pitsch presented an improved phase field LB model [18]. In [19] a lattice Boltzmann front-tracking method was introduced. A first local lattice Boltzmann method for immiscible fluids has been proposed in [20]. Here only the diffusive transport of an index function is considered and the resulting surface tension depends on the velocity. A local lattice Boltzmann method for multiple immiscible fluids and dense suspensions of drops has been proposed by Spencer et al. [21]. This approach defines a link phase field and uses it for a 'crude' local approximation of the gradient of the phase field. LB multiphase models have been extended and optimized and applied to the simulation of flows through porous media [6,22–29,13,30,31].

2.1. The D3Q13 model

The number of microscopic velocities, which define the 'lattice' in the LBM, depends on the transport problem to be simulated. A common labeling for different lattice Boltzmann models is **DxQb** [32], where **x** is the space dimension and **b** the number of microscopic velocities. To simulate Stokes problems in three dimensions D3Q13, D3Q15, D3Q19 and D3Q27 models are used, which have only next neighbor interaction. Adding more speeds improves the stability and accuracy of the models but also increases the computational requirements and the non-locality of the scheme. In the following discussion the font bold sans serif ($\mathbf{x}$) represents a three-dimensional vector in space and the font bold with serif $\boldsymbol{f}$ a b-dimensional vector, where b is the number of microscopic velocities. In the subsequent sections we describe the D3Q13 model which was introduced by d'Humières et al. in [33] and is probably the model with the minimal set of velocities in three dimensions to obtain the Stokes equations. It has the following microscopic velocities

$$\{\mathbf{e}_i \mid i = 0, \ldots, 12\} = \begin{Bmatrix} 0 & c & -c & c & -c & c & -c & c & -c & 0 & 0 & 0 & 0 \\ 0 & c & -c & -c & c & 0 & 0 & 0 & 0 & c & -c & c & -c \\ 0 & 0 & 0 & 0 & 0 & c & -c & -c & c & c & -c & -c & c \end{Bmatrix}, \tag{2}$$

where c is a constant microscopic speed. The microscopic velocities as shown in Fig. 1 define a computational lattice where a node is connected to neighboring nodes through the vectors $\{\Delta t\, \mathbf{e}_i \mid i = 0, \ldots, 12\}$. The time step Δt defines also the grid spacing by $h = c\Delta t$. If we relate the position of a node in the lattice through $x = h \times i$, $y = h \times j$, $z = h \times k$, where $i \in [1, nx]$, $j \in [1, nj]$ and $k \in [1, nz]$ are indices, a careful inspection of the connection graph of the lattice reveals that the lattice can be split into two totally independent sub-lattices consisting of the nodes with $x + y + z$ even for one and odd for the other [33]. So we use only the lattice composed of the nodes with $x + y + z$ even. The basic unit cell is a rhombic dodecahedron shown in Fig. 1. It is a Catalan solid with 12 rhombic faces, 24 edges and 14 vertices and defines a space filling lattice [34] as shown in Fig. 1. The vertices are given by $(\pm 1, \pm 1, \pm 1)h$, $(\pm 1, 0, 0)h$, $(0, \pm 1, 0)h$, $(0, 0, \pm 1)h$ and the volume of the unit cell $V = 2\,h^3$.

2.2. Two different lattice Boltzmann automata

We follow the idea of the multiphase model to have two different automata, one for the flow field and one for the advection of the phase field [17]. The phase field θ indicates the fluid phase: $\theta = -1$ for phase 1 and $\theta = 1$ for phase 2. The value of θ is constant in the bulk of each phase and varies only in the diffusive fluid–fluid interface. $\mathbf{C} = \nabla\theta$ is the gradient of the order parameter and the normalized gradient

$$\mathbf{n} = \frac{\mathbf{C}}{|\mathbf{C}|}, \tag{3}$$

defines the orientation of the fluid–fluid interface. The interfacial tension force is defined as a body force

$$\mathbf{f} = \sigma\,\kappa\,\mathbf{n}\delta_\Gamma, \tag{4}$$

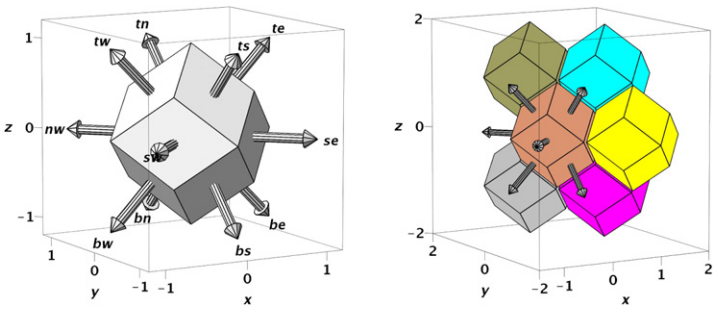

Fig. 1. Left: the unit cell for the D3Q13 model is a rhombic dodecahedron; right: rhombic dodecahedra honeycomb.

where σ is the coefficient of the interfacial tension, κ is the mean curvature, $\mathbf{n}$ is the normal to the fluid–fluid interface and δ_Γ is a delta function concentrated on the fluid–fluid interface. The interfacial tension can be represented as the divergence of a stress tensor T [35]

$$\mathbf{f} = \nabla \cdot \mathsf{T}, \qquad T_{\alpha\beta} = \sigma\, \delta_\Gamma \left(\delta_{\alpha\beta} - n_\alpha n_\beta\right), \tag{5}$$

where $\delta_{\alpha\beta}$ is the Kronecker symbol and $\alpha = x, y, z$, $\beta = x, y, z$. In the continuum limit we have the following relation

$$\mathbf{n}\, \delta_\Gamma = \frac{1}{2}\nabla\theta = \frac{1}{2}\frac{\nabla\theta}{|\nabla\theta|}|\nabla\theta| = \frac{1}{2}\,\mathbf{n}\,|\nabla\theta|. \tag{6}$$

Relation (5) will be used to integrate the interfacial tension forces in the LB scheme and relation (6) is needed for the derivation of the macroscopic multiphase equations.

The lattice Boltzmann equation for the flow field is given with

$$f_i(t + \Delta t, \mathbf{x} + \mathbf{e}_i \Delta t) = f_i(t, \mathbf{x}) + \Omega_i(\{f_j(t, \mathbf{x}), j = 0, \ldots, b-1\}, \mathbf{C}(t, \mathbf{x})), \quad i = 0, \ldots, b-1, \tag{7}$$

where $\{f_j, j = 0, \ldots, b-1\}$ are distributions (mass fractions) with unit kg m^{-3} propagating with microscopic velocities $\mathbf{e}_i$ and colliding at the lattice nodes $\mathbf{x}$. The collision operator Ω conserves mass and momentum.

The lattice Boltzmann equation for the advection of the phase field is given with

$$g_i\left(t + \frac{\Delta t}{2}, \mathbf{x} + \mathbf{e}_i \Delta t\right) = g_i\left(t - \frac{\Delta t}{2}, \mathbf{x}\right) + \Theta_i\left(\left\{g_j\left(t - \frac{\Delta t}{2}, \mathbf{x}\right), j = 0, \ldots, b-1\right\}, \mathbf{u}\left(t - \frac{\Delta t}{2}, \mathbf{x}\right)\right),$$
$$i = 0, \ldots, b-1, \tag{8}$$

where $\{g_j, j = 0, \ldots, b-1\}$ are distributions (unit-less fractions) of the phase field indicator function and $\mathbf{u}$ is the flow field. The collision operator Θ conserves the indicator function only.

The 'duty' of the LB automata for the phase field is to (a) keep interface sharp, (b) advect the phase field, (c) integrate the contact angle and (d) to compute gradients of the phase field locally. The 'duty' of the LB automata for the flow field is to (a) solve Stokes flow, (b) integrate capillary forces and (c) integrate the interface condition between the two fluids.

2.3. Moments of the distribution functions

The distributions $\{f_j, j = 0, \ldots, b-1\}$, $\{g_j, j = 0, \ldots, b-1\}$ can be transformed to moment space by building moments with respect to the microscopic velocity,

$$m_j = \sum_{i=0}^{b-1} Q_{j,i} f_i, \qquad m_j^\theta = \sum_{i=0}^{b-1} Q_{j,i}\, g_i, \quad i = 0, \ldots, b-1, \tag{9}$$

where $\boldsymbol{Q_j}$ is a vector defining the moment. The zeroth moment is the sum of the distributions and the corresponding vector $\boldsymbol{Q_0}$ is given below. The first moments $m_{\{1,2,3\}}$ and $n_{\{1,2,3\}}$ are defined by vectors ($\boldsymbol{Q_1} - \boldsymbol{Q_3}$). Higher order moments are build in a way that the vectors $\left\{\boldsymbol{Q_j} \mid j = 0 \ldots 12\right\}$ are orthogonal with respect to the inner product $\langle \boldsymbol{Q_k}, \boldsymbol{Q_l} \rangle$. This can be achieved

with a Gram–Schmidt orthogonalization procedure and the resulting vectors are given by d'Humières [33]

$$\begin{aligned}
Q_{0,i} &= 1,\\
Q_{1,i} &= e_{x,i},\\
Q_{2,i} &= e_{y,i},\\
Q_{3,i} &= e_{z,i},\\
Q_{4,i} &= \frac{13}{2}\,\mathbf{e}_i^2 - 12\,c^2,\\
Q_{5,i} &= 3\,e_{x,i}^2 - \mathbf{e}_i^2,\\
Q_{6,i} &= e_{y,i}^2 - e_{z,i}^2,\\
Q_{7,i} &= e_{x,i}\,e_{y,i},\\
Q_{8,i} &= e_{y,i}\,e_{z,i},\\
Q_{9,i} &= e_{x,i}\,e_{z,i},\\
Q_{10,i} &= e_{x,i}(e_{y,i}^2 - e_{z,i}^2),\\
Q_{11,i} &= e_{y,i}(e_{z,i}^2 - e_{x,i}^2),\\
Q_{12,i} &= e_{z,i}(e_{x,i}^2 - e_{y,i}^2),
\end{aligned} \tag{10}$$

where $\mathbf{e}_i^2 = (e_{x,i}^2 + e_{y,i}^2 + e_{z,i}^2)$. The transformation matrix M is composed of the eigenvectors $\left\{\boldsymbol{Q}_j \mid j = 0 \ldots 12\right\}$

$$\mathsf{M}_{ji} = Q_{j,i}. \tag{11}$$

The moments $\boldsymbol{m}$ (in vector notation) of the mass fractions are labeled as

$$\boldsymbol{m} = \mathsf{M}\boldsymbol{f} := \left(\rho, j_x, j_y, j_z, e, p_{xx}, p_{ww}, p_{xy}, p_{yz}, p_{xz}, h_x, h_y, h_z\right). \tag{12}$$

Moment ρ of zero order is the density variation around the reference density ρ_r and the moments ($j_x = \rho_r u_x$, $j_y = \rho_r u_y$, $j_z = \rho_r u_z$) of first order are the macroscopic momentum, where $\mathbf{u}$ is the macroscopic velocity. Moment e of second order corresponds to the microscopic kinetic energy and is related to the pressure, moments $p_{xx}, p_{ww}, p_{xy}, p_{yz}, p_{xz}$ of second order are related to the viscous stress tensor. Moments h_x, h_y, h_z of third order are related to second derivatives of the flow field.

The moments $\boldsymbol{m}^{\boldsymbol{\theta}}$ (in vector notation) of the fractions of the phase field are labeled as

$$\boldsymbol{m}^{\boldsymbol{\theta}} = \mathsf{M}\boldsymbol{g} := \left(\theta, j_x^\theta, j_y^\theta, j_z^\theta, e^\theta, p_{xx}^\theta, p_{ww}^\theta, p_{xy}^\theta, p_{yz}^\theta, p_{xz}^\theta, h_x^\theta, h_y^\theta, h_z^\theta\right). \tag{13}$$

Moment θ of zero order is the indicator function (phase field) and moments $(j_x^\theta, j_y^\theta, j_z^\theta)$ of first order are related to the gradient of the phase field. Moments $e^\theta, p_{xx}^\theta, p_{ww}^\theta, p_{xy}^\theta, p_{yz}^\theta, p_{xz}^\theta$ of second order are related to second order derivatives of the phase field, and moments h_x, h_y, h_z of third order are related to third order derivatives.

2.4. The collision operator for the flow field

The collision is done in moment space and given for the flow field by

$$\Omega = \mathsf{M}^{-1}\,\mathsf{S}\left(\boldsymbol{m} - \boldsymbol{m}^{eq}\right), \tag{14}$$

where the equilibrium moments are given with

$$\begin{aligned}
e^{eq} &= \left(\frac{39}{2}\,c_s^2 - 12\,c^2\right)\rho - \frac{13}{2}\,\sigma|\mathbf{C}|\\
p_{xx}^{eq} &= \sigma|\mathbf{C}|\frac{1}{2}(2\,{n_x}^2 - {n_y}^2 - {n_z}^2)\\
p_{ww}^{eq} &= \sigma|\mathbf{C}|\frac{1}{2}({n_y}^2 - {n_z}^2)\\
p_{xy}^{eq} &= \sigma|\mathbf{C}|\frac{1}{2}\,n_x\,n_y\\
p_{yz}^{eq} &= \sigma|\mathbf{C}|\frac{1}{2}\,n_y\,n_z\\
p_{xz}^{eq} &= \sigma|\mathbf{C}|\frac{1}{2}\,n_x\,n_z\\
h_{x,y,z}^{eq} &= 0.
\end{aligned} \tag{15}$$

σ is the value of the interfacial tension, c_s is the speed of sound and relates pressure and density variation, $\mathbf{C}$ is the gradient of the phase field and $\mathbf{n}$ the normalized gradient

$$n_\alpha = \frac{C_\alpha}{|\mathbf{C}|}. \tag{16}$$

The strength of this relaxation process is affected by the diagonal matrix S, where the elements are relaxation rates for the corresponding non-equilibrium moments:

$$\begin{aligned}
&s_{0,0} = s_{1,1} = s_{2,2} = s_{3,3} = 0\\
&s_{4,4} = s_e = -1\\
&s_{5,5} = s_{6,6} = s_{p_{xx}} = s_{p_{ww}} = -\frac{2}{8\frac{\nu}{c^2\Delta t} + 1}\\
&s_{7,7} = s_{8,8} = s_{9,9} = s_{p_{xy}} = s_{p_{yz}} = s_{p_{xz}} = -\frac{2}{4\frac{\nu}{c^2\Delta t} + 1}\\
&s_{10,10} = s_{11,11} = s_{12,12} = s_{h_z} = -2 - s_{p_{xx}},
\end{aligned} \tag{17}$$

where $\nu(\theta) = \mu/\rho_r$ is the kinematic viscosity of the fluids depending on the phase field value. The viscosity can be either a step function,

$$\nu = \begin{cases} \nu_1 & \text{if } \theta < 0,\\ \nu_2 & \text{else} \end{cases} \tag{18}$$

or a linear interpolation dependent on θ

$$\nu = \frac{(1+\theta)}{2}\nu_2 + \frac{(1-\theta)}{2}\nu_1. \tag{19}$$

The pressure variation is given by $p = c_s^2\rho$.

2.5. The collision operator for the phase field

The collision for the phase field is also done in moment space and given with

$$\Theta = \mathsf{M}^{-1}\boldsymbol{R}\{\boldsymbol{k}\} = \mathsf{M}^{-1}\boldsymbol{R}\left\{\mathsf{S}^\theta\left(\boldsymbol{m}^\theta - \boldsymbol{m}^{\theta,eq}\right)\right\}, \tag{20}$$

where the equilibrium moments $\boldsymbol{m}^{\theta,eq}$ are given with

$$j_x^{\theta,eq} = \theta\, ux \tag{21}$$

$$j_y^{\theta,eq} = \theta\, uy \tag{22}$$

$$j_z^{\theta,eq} = \theta\, uz \tag{23}$$

$$e^{\theta,eq} = p_{\alpha\beta}^{\theta,eq} = h_\alpha^{\theta,eq} = 0, \quad \alpha,\beta = x,y,z. \tag{24}$$

The strength of this relaxation process is affected by the diagonal matrix S^θ, where the elements are relaxation rates for the corresponding non-equilibrium moments:

$$s_x^\theta = s_y^\theta = s_z^\theta = -\frac{8}{4 + 13\frac{D}{c^2\Delta t}} \tag{25}$$

$$s_e^\theta = s_{p_{xx}}^\theta = s_{p_{ww}}^\theta = s_{p_{xy}}^\theta = s_{p_{yz}}^\theta = s_{p_{xz}}^\theta = -2 - s_x^\theta \tag{26}$$

$$s_{h_x}^\theta = s_{h_y}^\theta = s_{h_z}^\theta = s_x^\theta, \tag{27}$$

where D is the diffusivity, which is chosen in such a way that

$$s_x^\theta = s_y^\theta = s_z^\theta = -1. \tag{28}$$

The gradient of the phase field can be computed from the non-equilibrium part of the first order moment

$$\partial_\alpha\theta = C_\alpha = s_\alpha\frac{13}{8\,c^2\,\Delta t}(j_\alpha - \theta\, u_\alpha) = s_\alpha k_{j_\alpha}, \quad \alpha = x,y,z. \tag{29}$$

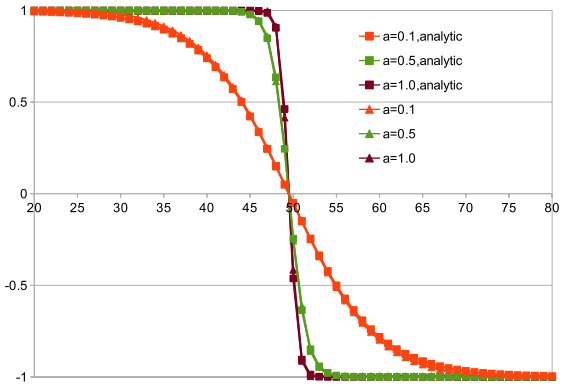

Fig. 2. Width of interface for different values of a_{sep}.

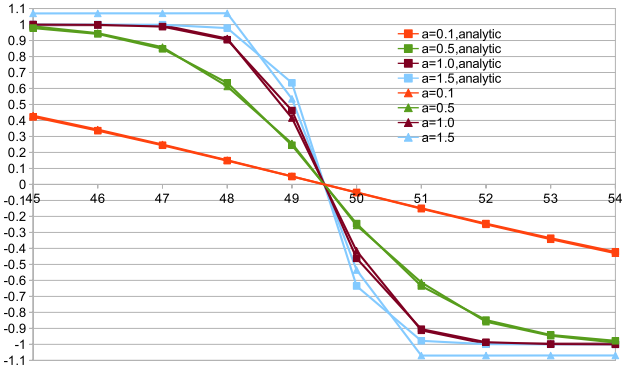

Fig. 3. Width of interface for different values of a_{sep}.

The operator R acts on the first order moments and keeps the interface sharp.

$$\begin{aligned}&\boldsymbol{R}\left\{0, k_{j_x}, k_{j_y}, k_{j_z}, k_e, k_{p_{xx}}, k_{p_{ww}}, k_{p_{xy}}, k_{p_{yz}}, k_{p_{xz}}, k_{h_x}, k_{h_y}, k_{h_z}\right\}\\&\quad=\left(0, k'_{j_x}, k'_{j_y}, k'_{j_z}, k_e, k_{p_{xx}}, k_{p_{ww}}, k_{p_{xy}}, k_{p_{yz}}, k_{p_{xz}}, k_{h_x}, k_{h_y}, k_{h_z}\right).\end{aligned}\tag{30}$$

The gradient of the phase field is adjusted in such a way that it has a steep slope if the phase field value is close to zero (the interface) and a slope of zero if it is close to minus or plus one. The direction of the gradient is kept:

$$|\mathbf{C}| = a_{sep} * (1 - \theta^2).\tag{31}$$

The constant a_{sep} is responsible for the sharpness of the interface. The larger a_{sep} the sharper the interface. The first order moments are modified through the following algorithm:

$$k'_{j_\alpha} = d\, k_{j_\alpha}\tag{32}$$

$$d = \begin{cases}\dfrac{a_{sep} * (1 - \theta^2)}{|\mathbf{C}|} & \text{if } |\mathbf{C}| > \epsilon\\ 1 & \text{else.}\end{cases}\tag{33}$$

We set $\epsilon = 1E - 6$ in all simulations. If we consider a flat interface orthogonal to the x-direction, Eq. (31) simplifies to $\partial_x\theta(x) = a_{sep} * (1 - \theta(x)^2)$. The solution is $\theta(x) = tanh(a_{sep}(x + c))$, where c is a constant indicating the location of the interface. In Figs. 2 and 3 the resulting shapes for a flat interface for different values of a_{sep} are given and compared to the analytic solution. The numerical solution is stable and once it has reached its final shape it does not change anymore, even after millions of iterations. The value of $a_{sep} = 1.5$ gives a strong separation, but induces some artifacts in the numerical solution, e.g.: the value outside the interface is larger than 1 and smaller than -1. We set $a_{sep} = 1$ in all subsequent simulations.

2.6. Boundary conditions

The boundary conditions are only discussed shortly, for details we refer to [36–38]. For the boundary conditions we assume that the boundary is located halfway between a solid site and a fluid site. The boundary conditions are then

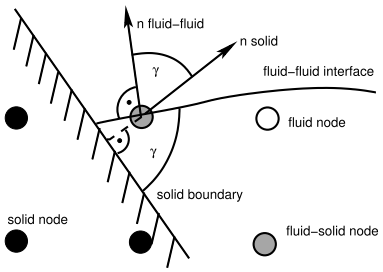

Fig. 4. The contact angle in the lattice Boltzmann method.

implemented through a modified collision operator on the solid site. The pressure boundary conditions for the flow field are implemented through the anti-bounce-back rule,

$$\Omega_i = \frac{1}{4c^2}\, p_{BC} - f_{\bar{i}}(t, \mathbf{x}), \tag{34}$$

where $f_{\bar{i}}$ is the anti-parallel distribution of f_i. Velocity boundary conditions are implemented through the bounce back rule:

$$\Omega_i = \frac{\rho_r}{4c^2}(\mathbf{e}_i\, \mathbf{u}_{BC}) + f_{\bar{i}}(t, \mathbf{x}). \tag{35}$$

For the phase field the concentration is prescribed by the anti-bounce-back rule,

$$\Theta_i = \frac{2}{13}\, \theta_{BC} - g_{\bar{i}}(t, \mathbf{x}), \tag{36}$$

and an impermeable wall is implemented through the following bounce back rule:

$$\Theta_i = g_{\bar{i}}(t, \mathbf{x}). \tag{37}$$

2.7. The static contact angle

In most LB models the contact angle is implemented in a nonlocal manner. It is prescribed either through a potential at the wall for the SC model [23,39,40], through a surface free energy density function in the FE model [41,42] or through prescribed phase densities at the wall for the RK model [43,44]. In [45] an improved method for the RK with slip boundary conditions has been developed. An implementation of the contact angle for a free surface LBM based on a local triangulation of the phase field has been developed in [46]. Dynamic contact angles are discussed e.g: in [41,47,42,48].

The contact angle for our LB method is implemented with a *local* algorithm as well. We compute or impose for each fluid node next to a solid node (meaning that the fluid node has a common link with a solid node a labeled hereafter fluid–solid node) a vector indicating the normal direction for the fluid–solid interface. If the geometry is given in form of a voxel matrix, the normal pointing in the fluid domain can be approximated by

$$\mathbf{v}_S(\mathbf{x}) = \sum_{i=1}^{b-1} \frac{\mathbf{e}_i}{c^2}\phi\,(\mathbf{x} + \mathbf{e}_i \Delta t) \tag{38}$$

$$\mathbf{n}_S = \frac{\mathbf{v}_S}{|\mathbf{v}_S|} \tag{39}$$

where $\phi = 1$ for a fluid and fluid–solid node and $\phi = 0$ otherwise. The idea is to adjust the normal of the fluid–fluid interface given by Eq. (29) in such a way, that the imposed contact angle γ is respected as depicted in Fig. 4.

We can modify the three first order moments ((21)–(23)) of the phase field to adjust the contact angle without modifying the mass balance for the phase field, and we have therefor three unknowns. The first constraint is that the contact angle is respected:

$$equ1(C_x, C_y, C_z) := C_\alpha n_{S,\alpha} - \cos\gamma = 0. \tag{40}$$

The second constraint is that the interface is kept sharp. The amplitude of the gradient of the phase field is adjusted in the same way as in Eq. (31).

$$equ2(C_x, C_y, C_z) := |\mathbf{C}| - a_{sep} * (1 - \theta^2) = 0. \tag{41}$$

As third constraint we choose to minimize the modification to the previous state:

$$fun(C_x, C_y, C_z) = |\mathbf{C} - \mathbf{C}^{old}|. \tag{42}$$

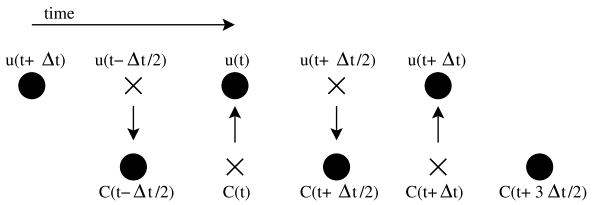

Fig. 5. The staggered algorithm for flow and phase fields.

The problem can be formulated as a constraint nonlinear optimization with Lagrange multiplier λ_i:

$$\Lambda(C_x, C_y, C_z, \lambda_1, \lambda_2) = fun + \lambda_1\, equ1 + \lambda_2\, equ2. \tag{43}$$

Minimizing $\Lambda(C_x, C_y, C_z, \lambda_1, \lambda_2)$ leads to a (local) nonlinear equation system with 5 unknowns, which can be solved efficiently with a Newton–Raphson method. The first order moments j_α^θ are then adjusted in the collision operator using Eq. (29).

2.8. Overall algorithm

We use a staggered time stepping (see Eqs. (7) and (8)) to compute the coupled problem of flow and advection of the phase field. The gradient at time step t is computed by $\mathbf{C}(t) = \frac{1}{2}\left(\mathbf{C}(t + \frac{\Delta t}{2}) + \mathbf{C}(t - \frac{\Delta t}{2})\right)$. The flow velocity at time step $t - \frac{\Delta t}{2}$ is computed by $\mathbf{u}(t) = \frac{1}{2}\left(\mathbf{u}(t - \Delta t) + \mathbf{u}(t)\right)$.

The staggered algorithm is depicted in Fig. 5.

2.9. Macroscopic equations

With a multi-scale analysis in space and time called Chapman–Enskog expansion, which was developed by Enskog [49] (a little bit earlier Chapman [50] had given formulas for the coefficient of thermal conduction and the viscosity by a different technique) to derive solutions for the Boltzmann equation [51], it is possible to show that LBE leads to the incompressible Navier–Stokes equations [52,53]. An alternative method of deriving the macroscopic equation for the LBE is an asymptotic analysis as performed in [54,55]. While most of the LBM models for multiphase and multi-component fluid flows are based on heuristic ideas with no direct connection to kinetic theory, Luo [56,57] and Luo and Girimaji [58,59] have rigorously derived the LBM models for multiphase fluids from the Enskog equation and for multi-component fluids from the corresponding kinetic equations. A strict derivation for RK type models is given in the PhD thesis of Kehrwald [60] and in [15]. A derivation of the macroscopic equations for the present model is given in the Appendix.

3. Examples

In all subsequent simulations we set the microscopic velocity to $c = 1\ \frac{\mathrm{m}}{\mathrm{s}}$, the reference density to $\rho_r = 1\ \frac{\mathrm{kg}}{\mathrm{m}^3}$, the grid spacing to $h = 1$ m and the speed of sound to $c_s = \frac{1}{\sqrt{3}}\ \frac{\mathrm{m}}{\mathrm{s}}$. All simulations are performed in single precision.

3.1. A static bubble

In this subsection we validate the equation of Young–Laplace $\Delta p_a = \frac{2\sigma}{r}$ for a bubble of radius r. The domain is a box of size $5 \times r$, the interfacial tension is $\sigma = 0.05\ \frac{\mathrm{N}}{\mathrm{m}}$, the dynamic viscosity of both phases is $\mu = 0.05$ Pa s. The simulation is run until a steady state is reached and the phase field does not move and the pressure does not change with time anymore. The simulations were run for millions of iterations to check whether the bubble is dissolving. In all cases the bubble kept its shape. The error is defined by $error = \frac{|\Delta p_a - \Delta p_{sim}|}{\Delta p_a}$, where the pressure is computed by averaging the pressures in both phases where $|\theta| > 0.99$. The radius is computed by fitting a sphere to the iso-surface $\theta = 0$. The spurious currents are computed by an averaged velocity in the interface where $|\theta| < 0.99$. In Table 1 the results for different radii are shown. Especially for very small radii the results are very favorable.

The spurious currents are of order $0.01\,\sigma/\mu$ as observed in [35,61]. In Table 2 the spurious currents are evaluated for different values of the interfacial tension for a bubble of radius $r = 7.49$ m and a dynamic viscosity of $\mu = 0.05$ Pa s for both phases. In Fig. 6 the shape of a bubble with $\sigma = 0$ N/m and with $\sigma = 0.05$ N/m is shown in black. The case with no interfacial tension shows slight deviations from the shape of a circle, which is shown in gray color for comparison.

In Fig. 7 the error for a bubble of radius $r = 7.5$ m is shown for different values of the inner and outer viscosities and interfacial tension. The results show that the approach works for large viscosity ratios over a wide range of surface tension values. As soon as the interfacial tension surpasses the value of the lowest dynamic viscosity, the spurious currents and the error increase significantly. This limits the possible ratio between σ/μ_{lowest} to a certain threshold. Spurious currents

Table 1
Error in pressure for a static bubble with different radii.

Radius r (m)	Error (–)	Spurious current (m/s)
2.30	0.039	6.0E−3
2.80	0.021	5.4E−3
3.30	0.005	4.8E−3
7.49	0.014	4.5E−3
15.62	0.011	4.9E−3
31.68	0.011	5.2E−3

Table 2
Error in pressure and spurious current for a static bubble of radius $r = 7.49$ with varying interfacial tension.

σ (N/m)	Error (–)	Spurious current (m/s)
0.0	0.0	0.0
0.0005	0.012	1.1E−4
0.005	0.008	5.8E−4
0.05	0.014	4.9E−3

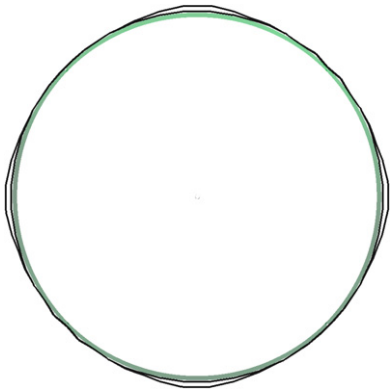

Fig. 6. Shape of a bubble of radius 7.5 m with $\sigma = 0$ N/m, $\sigma = 0.05$ N/m and a circle for comparison.

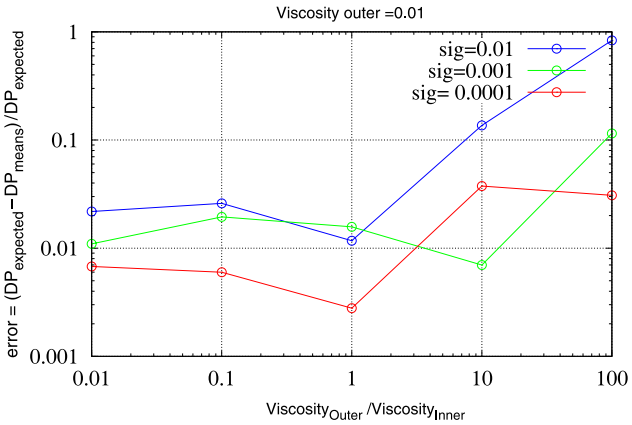

Fig. 7. Error in pressure for a bubble of radius 7.5 m with different values of viscosities and interfacial tension.

are induced through two mechanisms: the first one is that the algorithm does not have an inherent force balance [62]. The second one is that the numerical model only approximates the exact location of the interface and therefor has errors in the curvature estimates. Especially for large ratios of σ/μ this effect is very serious [62]. LB models that reduce or eliminate spurious currents have been proposed [63–72]. A general method for the reduction of spurious currents can be found in [73]. A challenging problem is to reduce the spurious currents due to an insufficient approximation of the curvature of the phase field and has been covered by e.g.: [62,74–77].

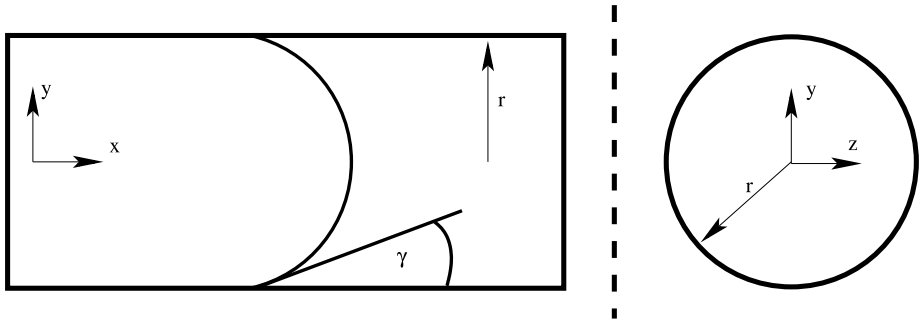

Fig. 8. A closed capillary tube to test the contact angle.

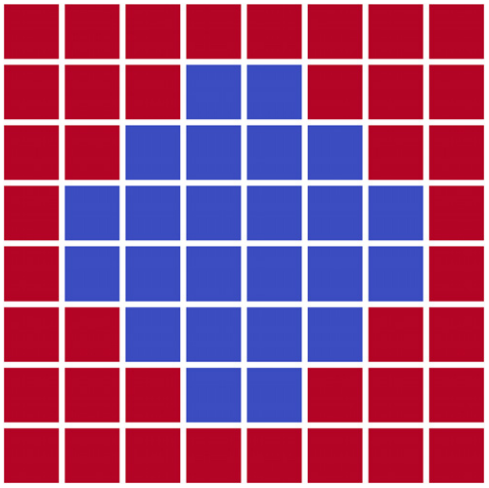

Fig. 9. Discretized mesh for a circular pipe, 24 fluid cells.

3.2. A closed capillary tube

In Fig. 8 the setup for testing the contact angle is shown. It is a circular pipe along the x-axes which is filled initially with one fluid in the first half of the x-direction and with the other fluid in the second half. The simulation is run until a steady state is reached and the phase field does not move and the pressure does not change with time anymore. The theoretical pressure jump can be computed by the equation of Young–Laplace $\Delta p_a = \frac{2\sigma \cos\gamma}{r}$, where γ is the contact angle. The error is defined by $error = \frac{|\Delta p_a - \Delta p_{sim}|}{\Delta p_a}$. The pressure and the value for the spurious current are computed as in the previous example. The actual radius is computed by equating the area of the nodes occupied by fluid and fluid–solid cells in a cross section to the area of a circle. As an example the number of fluid cells is 24 in Fig. 9 and the radius is computed as $r = \sqrt{24m^2/\pi} \approx 2.76$ m. The length of the domain in x-direction is $4 \times r$. In Table 3 the results for a fixed contact angle of $\gamma = 60^\circ$ for different radii r, for different values of interfacial tension σ and dynamic viscosities $\mu_1 = \mu_2$ are given. Even for a very coarse resolution as depicted in Fig. 9 the method gives a stable interface and reasonable results.

In Fig. 10 the results for a radius $r = 11.73$ m, a fixed dynamic viscosity $\mu_1 = 0.01$ Pa s, an interfacial tension of $\sigma = 0.01$ N/m and for different contact angles and viscosities μ_2 are shown. The results show that the approach works for large viscosity ratios over a wide range of surface tension values. Again, the error increases if the ratio of $\sigma/\mu_{smallest}$ is larger than one.

3.3. Annular flow between two concentric cylinders

In this section we investigate different viscosity ratios. The setup is shown in Fig. 11. The cross section perpendicular to the flow direction are two concentric circles with radii r_1 and r_3 and the flow domain is in between. At both circles a velocity boundary condition is prescribed. The interface between the fluids is at location r_2. If the flow and the interface are stable

Table 3
Error in pressure for a closed capillary tube for $\gamma = 60°$ and different values for r, σ and μ.

Radius r (m)	σ (N/m)	$\mu_1 = \mu_2$ (Pa s)	Error (–)	Spurious current (m/s)
2.76	0.1	0.1	0.11	4.92E−3
2.76	0.01	0.01	0.31	5.43E−3
2.76	0.001	0.001	0.31	5.43E−3
5.97	0.1	0.1	0.13	3.97E−3
5.97	0.01	0.01	0.14	4.21E−3
5.97	0.001	0.001	0.15	4.17E−3
12.41	0.1	0.1	0.06	3.44E−3
12.41	0.01	0.01	0.06	3.30E−3
12.43	0.001	0.001	0.06	3.33E−3
25.18	0.1	0.1	0.06	3.25E−3
25.18	0.01	0.01	0.06	3.28E−3
25.18	0.001	0.001	0.06	3.24E−3

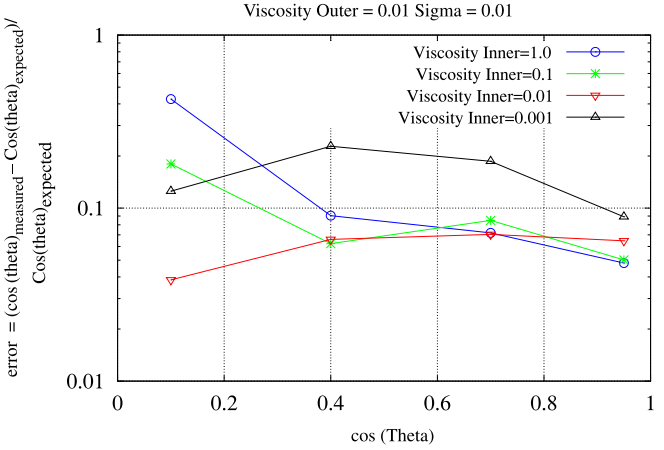

Fig. 10. Error in pressure for a closed capillary tube for different values of viscosities and interfacial tension.

the analytic solution is given by

$$u_{inner} = \frac{u_1 \mu_1 \ln \frac{r_2}{r_3} + \mu_2 \left(u_1 \ln \frac{r}{r_2} + u_3 \ln \frac{r_1}{r} \right)}{\mu_1 \ln \frac{r_2}{r_3} + \mu_2 \ln \frac{r_1}{r_2}} \tag{44}$$

$$u_{outer} = \frac{u_3 \mu_2 \ln \frac{r_1}{r_2} + \mu_1 \left(u_1 \ln \frac{r}{r_3} + u_3 \ln \frac{r_2}{r} \right)}{\mu_1 \ln \frac{r_2}{r_3} + \mu_2 \ln \frac{r_1}{r_2}} \tag{45}$$

$$u = \begin{cases} u_{inner} & \text{if } r < r_2, \\ u_{outer} & \text{else.} \end{cases} \tag{46}$$

The goal of this chapter is to test the method for different viscosity ratios and not to study the stability of this flow. Extensive numerical studies of annular flow can be found e.g.: in [78–80]. Modeling of flow pattern transitions in concentric annuli can be found in [81]. For Stokes flow in a pipe core annular flow is always instable to long waves and stable for short waves [79]. We choose a very short domain with periodic boundary conditions and low interfacial tension to avoid instability. In Fig. 12 the numerical solution (symbols) along the z-axis is plotted against the analytical solution (line) for $u_1 = -0.05$ m/s, $u_2 = 0.05$ m/s, $r1 = 12.5$ m, $r2 = 20.5$ m and $r3 = 28.5$ m. The outer dynamic viscosity is $\mu_2 = 0.1$ Pa s and the inner viscosity $\mu_1 = 0.1, 0.01, 0.001$ Pa s. The interfacial tension is set to $\sigma = 1E{-}6$ N/m.

4. Conclusions

We have proposed and analyzed a lattice Boltzmann model for immiscible two-phase Stokes flow with a local collision operator. A new method for keeping the interface sharp and for implementing the contact angle locally has been presented. The method allows an independent adjustment of surface tension and viscosities. The sharpness of the interface is 2–3 lattice nodes and does not depend on the value of the surface tension or the viscosities. The method works for a wide range of parameters. No lattice pinning has been observed in this method. Especially for a coarse grid resolution the method gives good results. The relative error in the pressure jump for a bubble approximated with less than 5 grid points is below

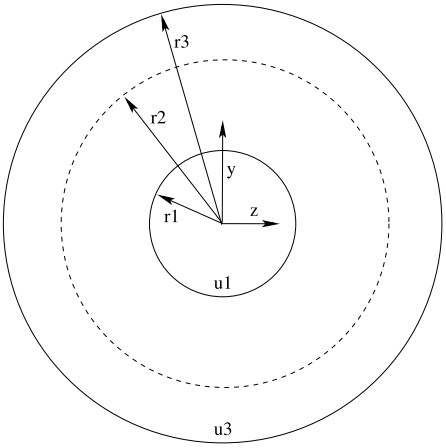

Fig. 11. The setup for two-phase flow between two concentric pipes with boundary conditions.

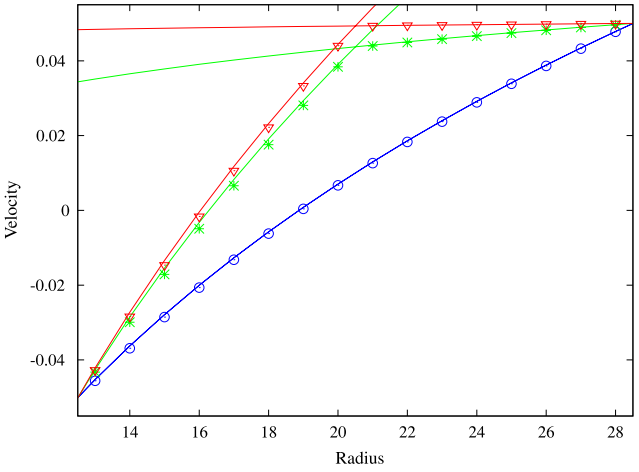

Fig. 12. The velocity in the flow direction for multiphase flow in a concentric annulus with different values of viscosities and interfacial tension, blue (circles) is viscosity ratio 1, green (crosses) is 10 and red (triangles) is 100.

0.05. Spurious currents are observed and further investigation is needed, whether it is possible to eliminate them while maintaining a local collision operator. We presented only steady state results, transient testcases like a capillary wave will be presented in a forthcoming paper. Since the method has a local collision operator, it is very suitable for a parallel implementation.

Appendix A. Derivation of macroscopic equations by asymptotic analysis

The derivation of the resulting macroscopic equations is done either by a Chapman–Enskog analysis [53] or by an asymptotic analysis [54,55] or by using recurrence equations [37]. Here we use a procedure where the Mach number $\mathrm{Ma}_{LB} = u_{ref}/c$ is simultaneously lowered with increasing mesh resolution to obtain the macroscopic equations for the low Mach number limit (diffusive scaling). We use the scaling $c = c_r h_r/h$, where c_r and h_r are a fixed reference velocity and length, and $h = c\Delta t$ is the mesh spacing. The relation between the time step Δt and h is

$$\Delta t = \frac{h^2}{c_r h_r}. \tag{A.1}$$

The procedure is as follows:

A Taylor expansion of the left hand side of Eq. (7) or (8) in space and time up to a certain order
B Substitution of the mass fractions f_i by expressions in moments
C Transformation of the resulting equation system in moment space by multiplying matrix (11) from the left side
D Expansion of the moments of the resulting equation system in asymptotic series
E Collection of equations of the same order, starting with the lowest order

A: Taylor expansion

Using the relation (A.1), Eq. (7) is

$$f_i\left(t_n+\frac{h^2}{c_r h_r},\mathbf{x}+\hat{\mathbf{e}}_i h\right)-f_i(t,\mathbf{x})=\Omega_i\quad i=0,\ldots,12, \tag{A.2}$$

where $\hat{\mathbf{e}}_i=\mathbf{e}_i/c$ are the direction vectors of the discrete lattice. For athermal models where the speed of sound is constant, it is sufficient to do a Taylor expansion up to third order to obtain the Stokes equations. The Taylor expansion of the left hand side of Eq. (A.2) is [55]

$$\begin{aligned}f_i\left(t_n+\frac{h^2}{c_r h_r},\mathbf{x}_j+\hat{\mathbf{e}}_i h\right)-f_i\left(t,\mathbf{x}_j\right) &= h\left(\hat{\mathbf{e}}_i\cdot\nabla\right)f_i\left(t_n,\mathbf{x}_j\right)+h^2\left(\frac{1}{c_r h_r}\partial_t+\frac{1}{2}\left(\hat{\mathbf{e}}_i\cdot\nabla\right)^2\right)f_i\left(t_n,\mathbf{x}_j\right)\\ &\quad+h^3\left(\frac{1}{c_r h_r}\partial_t\left(\hat{\mathbf{e}}_i\cdot\nabla\right)+\frac{1}{6}\left(\hat{\mathbf{e}}_i\cdot\nabla\right)^3\right)f_i\left(t_n,\mathbf{x}_j\right)+\cdots\\ &=\sum_{k=1}^{\infty}h^k T_k\left(\frac{\partial_t}{c_r h_r},\left(\hat{\mathbf{e}}_i\cdot\nabla\right)\right)f_i\left(t_n,\mathbf{x}_j\right),\end{aligned} \tag{A.3}$$

where

$$T_k[a,b]=\sum_{2m+n=k}\frac{a^m\,b^n}{m!\,n!}. \tag{A.4}$$

We define the vector $\boldsymbol{V}$ as

$$V_i=\sum_{k=1}^{\infty}h^k\,T_k\left[\frac{\partial_t}{c_r h_r},\left(\hat{\mathbf{e}}_i\cdot\nabla\right)\right]f_i(t_n,\mathbf{x}_j),\quad i=0,\ldots,12. \tag{A.5}$$

B: Substitution of mass fractions by moments

The mass fractions in Eq. (A.5) are substituted by $\boldsymbol{f}=\mathsf{M}^{-1}\boldsymbol{m}$, where we use the scaling $c=c_r h_r/h$ in the entries of the matrix.

C: Transformation of the LB equation in moment space

We substitute the left hand side of the equation system (A.2) by Eq. (A.5) and multiply matrix (11) from the left side to obtain the equation system $\boldsymbol{EQ}$

$$\boldsymbol{EQ}\;:=\;\mathsf{M}\boldsymbol{V}-\mathsf{S}\left(\boldsymbol{m}-\boldsymbol{m}^{eq}\right)=\mathbf{0}. \tag{A.6}$$

Here we use the scaling $c=c_r h_r/h$ again in the entries of the matrix M.

D: Asymptotic expansion of moments

To analyze the complex system (A.6) of partial differential equations, we perform an asymptotic expansion of the moments. One has to expand the moments up to third order to obtain the macroscopic equations:

$$m_i(t,\mathbf{x})=m_{i,0}(t,\mathbf{x})+\frac{h}{h_r}m_{i,1}(t,\mathbf{x})+\left(\frac{h}{h_r}\right)^2 m_{i,2}(t,\mathbf{x})+\left(\frac{h}{h_r}\right)^3 m_{i,3}(t,\mathbf{x})+\mathcal{O}(h^4),\quad i=0,\ldots,12. \tag{A.7}$$

E1: Sorting equations order by order for the advection equation

The previous analysis is applied to Eq. (8) instead to Eq. (7), distributions f are replaced with distributions g and moments m with m^{θ}. We substitute expansion (A.7) in system (A.6) and collect the equations corresponding to the order in h. The lowest order is h^0 and appears in $EQ(1)-EQ(12)$ (where $EQ(1)$ means the second equation of the system (A.6)). $EQ(0)$ starts with order h^2.

First order moments

Order h^0 of $EQ\,(1) - EQ\,(3)$ yield the relation between first order moments and the derivative of θ:

$$\partial_\alpha \theta_0 = \frac{13\, s_\alpha}{8\, c_r\, h_r} \left(j^\theta_{\alpha,0} - \theta_0\, u_{\alpha,0} \right), \quad \alpha = x, y, z. \tag{A.8}$$

Order h^1 of $EQ\,(1) - EQ\,(3)$ yields the same relationship:

$$\partial_\alpha \theta_1 = \frac{13\, s_\alpha}{8\, c_r\, h_r} \left(j^\theta_{\alpha,1} - \theta_1\, u_{\alpha,1} \right), \quad \alpha = x, y, z. \tag{A.9}$$

With these relations the derivative of θ can be approximated up to second order by adding the two Eqs. (A.8) and (A.9), $\theta = \theta_0 + \frac{h}{h_r}\theta_1 + \mathcal{O}(h^2)$, and using $j_\alpha = j_{\alpha,0} + \frac{h}{h_r} j_{\alpha,1} + \mathcal{O}(h^2)$:

$$\partial_\alpha \theta = \frac{13\, s_\alpha}{8\, c_r\, h_r} \left(j^\theta_\alpha - \theta\, u_\alpha \right) + \mathcal{O}(h^2), \quad \alpha = x, y, z. \tag{A.10}$$

Second order moments

Order h^0 and h^1 of $EQ\,(4) - EQ\,(9)$ leads to a relationship between the second order moments and the second derivatives of θ_m, $m = 0, 1$. Using

$$m^\theta = m^\theta_0 + \frac{h}{h_r} m^\theta_1 + \mathcal{O}(h^2) \tag{A.11}$$

for the moments in general leads to the following relations

$$\begin{aligned}
\partial_{x,x}\,\theta &= \frac{13\, s_x}{12\, h_r^2\, c_r^2\, (2 + s_x)} \left(-3\, h_r\, c_r\, \partial_x\, (\theta\, u_x) + s_e\, e + 2\, s_{p_{xx}}\, p_{xx} \right) + \mathcal{O}(h^2) \\
\partial_{y,y}\,\theta &= \frac{13\, s_y}{12\, h_r^2\, c_r^2\, \left(2 + s_y\right)} \left(-3\, h_r\, c_r\, \partial_x\, \left(\theta\, u_y\right) + s_e\, e - s_{p_{xx}}\, p_{xx} + 3\, s_{p_{ww}}\, p_{ww} \right) + \mathcal{O}(h^2) \\
\partial_{z,z}\,\theta &= \frac{13\, s_z}{12\, h_r^2\, c_r^2\, (2 + s_z)} \left(-3\, h_r\, c_r\, \partial_x\, (\theta\, u_z) + s_e\, e - s_{p_{xx}}\, p_{xx} - 3\, s_{p_{ww}}\, p_{ww} \right) + \mathcal{O}(h^2) \\
\partial_{x,y}\,\theta &= \frac{-13\, s_x\, s_y}{8\, h_r^2\, c_r^2\, \left(s_x + s_y + s_x\, s_y\right)} \left(h_r\, c_r \left(\partial_y\, (\theta\, u_x) + \partial_x\, \left(\theta\, u_y\right) \right) - 2\, s_{p_{xy}}\, p_{xy} \right) + \mathcal{O}(h^2) \\
\partial_{y,z}\,\theta &= \frac{-13\, s_y\, s_z}{8\, h_r^2\, c_r^2\, \left(s_y + s_z + s_y\, s_z\right)} \left(h_r\, c_r \left(\partial_z\, \left(\theta\, u_y\right) + \partial_y\, (\theta\, u_z) \right) - 2\, s_{p_{yz}}\, p_{yz} \right) + \mathcal{O}(h^2) \\
\partial_{x,z}\,\theta &= \frac{-13\, s_x\, s_z}{8\, h_r^2\, c_r^2\, (s_x + s_z + s_x\, s_z)} \left(h_r\, c_r\, (\partial_z\, (\theta\, u_x) + \partial_x\, (\theta\, u_z)) - 2\, s_{p_{xz}}\, p_{xz} \right) + \mathcal{O}(h^2).
\end{aligned} \tag{A.12}$$

Note that with Eqs. (A.10) and (A.12) it is possible to compute the curvature of the phase field locally, if we assume that the divergence of **u** goes to zero.

The advection –diffusion equation

Collecting order h^2 and h^3 of $EQ\,(0)$ yields the following equation:

$$\partial_t\, \theta_m + \partial_\alpha\, j^\theta_\alpha + \partial_\alpha\, \partial_\alpha\, \theta_m, \quad m = 0, 1. \tag{A.13}$$

If we substitute the relations for the second order moments (A.8) and (A.9) in Eq. (A.13), use relation (A.11) and assume that the divergence of **u** goes to zero, we obtain

$$\partial_t\, \theta + u_\alpha\, \partial_\alpha\, \theta + c_r\, h_r \sum_{\alpha = x,y,z} \left(\left(\frac{4}{13} + \frac{8}{13\, s_\alpha} \right) \partial_{\alpha,\alpha}\, \theta \right) + \mathcal{O}(h^2). \tag{A.14}$$

The diffusion coefficient is given with Eq. (25). The collision rates (26) and (27) for the higher order moments are not relevant for the limit of the advection–diffusion equation and can be chosen in the range $]0, 2[$. The optimal values for the MRT model depend on the specific system under consideration (geometry, initial and boundary conditions) and are discussed extensively in the work of I. Ginzburg [38,82,37,83–85]. In [37] a magic combination for even (second order moments) and odd (first and third order moments) relaxation rates is given: $(\frac{1}{2} + \frac{1}{s_{even}})(\frac{1}{2} + \frac{1}{s_{odd}}) = const$. We choose the value $const = \frac{1}{4}$, so that $s_{even} + s_{odd} = -2$.

E2: Sorting equations order by order for the flow equation

We substitute expansion (A.7) in system (A.6) and collect the equations corresponding to the order in h. The lowest order is h^{-2} and appears in $EQ(4)$ (where $EQ(4)$ means the fifth equation of the system (A.6)). $EQ(1) - EQ(3)$ and $EQ(5) - EQ(12)$ start with order h^0 and $EQ(0)$ starts with order h^2.

Constant density

We have to start the analysis from the lowest order: Orders h^{-2} and h^{-1} of $EQ(4)$ yield

$$\rho_0 = 0, \ \rho_1 = 0. \tag{A.15}$$

Density fluctuations appear not until in the second order function ρ_2 and are related to the pressure field. This is consistent with the assumption of an incompressible flow field with constant density.

Second order moments related to the strain rate tensor

Order h^0 and h^1 of $EQ(1) - EQ(3)$ are zero if we substitute (A.15), but $EQ(4) - EQ(9)$ yield the relation between the zeroth and first term ($m = 0, 1$) of the second order moments expansion and the flow field $\mathbf{u}$:

$$e_m = \left(\frac{39}{2}c_s^2 - 12c_r^2\right)\rho_{m+2} + \frac{h_r\, c_r\, \rho_r}{s_e}\left(\partial_x u_{x,m} + \partial_y u_{y,m} + \partial_z u_{z,m}\right) - \frac{13}{2}\sigma|\mathbf{C}| \tag{A.16}$$

$$p_{xx,m} = \frac{h_r\, c_r\, \rho_r}{2\, s_{p_{xx}}}\left(2\,\partial_x u_{x,m} - \partial_y u_{y,m} - \partial_z u_{z,m}\right) + \sigma|\mathbf{C}|\,\frac{1}{2}(2\,{n_x}^2 - {n_y}^2 - {n_z}^2) \tag{A.17}$$

$$p_{ww,m} = \frac{h_r\, c_r\, \rho_r}{2\, s_{p_{ww}}}\left(\partial_y u_{y,m} - \partial_z u_{z,m}\right) + \sigma|\mathbf{C}|\,\frac{1}{2}({n_y}^2 - {n_z}^2) \tag{A.18}$$

$$p_{xy,m} = \frac{h_r\, c_r\, \rho_r}{2\, s\prime_{p_{xy}}}\left(\partial_y u_{x,m} + \partial_x u_{y,m}\right) + \sigma|\mathbf{C}|\,\frac{1}{2}\,n_x\, n_y \tag{A.19}$$

$$p_{yz,m} = \frac{h_r\, c_r\, \rho_r}{2\, s\prime_{p_{yz}}}\left(\partial_z u_{y,m} + \partial_y u_{z,m}\right) + \sigma|\mathbf{C}|\,\frac{1}{2}\,n_y\, n_z \tag{A.20}$$

$$p_{xz,m} = \frac{h_r\, c_r\, \rho_r}{2\, s\prime_{p_{xz}}}\left(\partial_z u_{x,m} + \partial_x u_{z,m}\right) + \sigma|\mathbf{C}|\,\frac{1}{2}\,n_x\, n_z. \tag{A.21}$$

Adding Eq. (A.16) for $m = 0, 1$ and taking into account the incompressibility condition (A.26) we obtain a second order approximation of the moment e

$$e_0 + h\, e_1 + \mathcal{O}(h^2) = e + \mathcal{O}(h^2) = \left(\frac{39}{2}c_s^2 - 12c_r^2\right)(\rho_2 + h\,\rho_3) - \frac{13}{2}\sigma|\mathbf{C}|. \tag{A.22}$$

Moment e is equal to e^{eq} up to second order and related to the pressure field through the density fluctuation ρ. If we relate the density variation to the pressure by $p = c_s^2(\rho_2 + h\,\rho_3) + \mathcal{O}(h^2)$, we can compute the pressure in the following way:

$$p = \frac{8}{13}\,c_r^2(\rho_2 + h\,\rho_3) + \frac{1}{3}\,\sigma|\mathbf{C}| - \frac{2}{39}e + \mathcal{O}(h^2). \tag{A.23}$$

With Eqs. (A.16)–(A.21) we can compute the elements of the strain rate tensor $\epsilon_{\alpha\beta} = \frac{1}{2}(\partial_\beta u_\alpha + \partial_\alpha u_\beta)$ in the same way. We set $s_{p_{xx}} = s_{p_{ww}} = s_\nu$ and $s_{p_{xy}} = s_{p_{yz}} = s_{p_{xz}} = s\prime_\nu$:

$$\begin{aligned}
\epsilon_{xx} &= \frac{s_\nu}{c_r\, h_r\, \rho_r}\left(\sigma\,|\mathbf{C}|\left(\frac{1}{3} - n_x^2\right) + \frac{2}{3}\,p_{xx} + \mathcal{O}(h^2)\right)\\
\epsilon_{yy} &= \frac{s_\nu}{c_r\, h_r\, \rho_r}\left(\sigma\,|\mathbf{C}|\left(\frac{1}{3} - n_y^2\right) - \frac{1}{3}\,p_{xx} + p_{ww} + \mathcal{O}(h^2)\right)\\
\epsilon_{zz} &= \frac{s_\nu}{c_r\, h_r\, \rho_r}\left(\sigma\,|\mathbf{C}|\left(\frac{1}{3} - n_z^2\right) - \frac{1}{3}\,p_{xx} - p_{ww} + \mathcal{O}(h^2)\right)\\
\epsilon_{xy} &= \frac{s\prime_\nu}{c_r\, h_r\, \rho_r}\left(p_{xy} - \frac{1}{2}\sigma\,|\mathbf{C}|\,n_x\, n_y\right) + \mathcal{O}(h^2)\\
\epsilon_{yz} &= \frac{s\prime_\nu}{c_r\, h_r\, \rho_r}\left(p_{yz} - \frac{1}{2}\sigma\,|\mathbf{C}|\,n_y\, n_z\right) + \mathcal{O}(h^2)\\
\epsilon_{xz} &= \frac{s\prime_\nu}{c_r\, h_r\, \rho_r}\left(p_{xz} - \frac{1}{2}\sigma\,|\mathbf{C}|\,n_x\, n_z\right) + \mathcal{O}(h^2).
\end{aligned} \tag{A.24}$$

Divergence free flow field

Collecting order h^2 and h^3 of $EQ\,(0)$ gives

$$\partial_x u_{x,m} + \partial_y u_{y,m} + \partial_z u_{z,m} = 0, \quad m = 0, 1. \tag{A.25}$$

Adding both equations gives

$$\partial_x u_x + \partial_y u_y + \partial_z u_z = \mathcal{O}(h^2). \tag{A.26}$$

Momentum conservation

Collecting and adding order h^2 and h^3 of $EQ\,(1)$ yields the momentum equation in x-direction. If we substitute the relations for the second order moments ((A.16)–(A.21)), we obtain after some algebra

$$\begin{aligned}\partial_t u_x + \frac{c_s^2}{\rho_r}\partial_x \rho - \frac{\sigma}{2\,\rho_r}\left(\partial_x \left(\left(1 - n_x^2\right)|\mathbf{C}|\right) - \partial_y \left(n_x n_y |\mathbf{C}|\right) - \partial_z \left(n_x n_z |\mathbf{C}|\right)\right) \\ \times \left(\frac{h_r c_r}{2\,s_\nu} - \frac{h_r c_r}{2\,s\prime_\nu}\right)\partial_{x,x} u_x + \left(\frac{h_r c_r}{4} + \frac{h_r c_r}{2\,s\prime_\nu}\right)\left(\partial_{y,y} u_x + \partial_{z,z} u_x\right) = \mathcal{O}(h^2).\end{aligned} \tag{A.27}$$

Collecting and adding order h^2 and h^3 of $EQ\,(2)$ yields the momentum equation in y-direction:

$$\begin{aligned}\partial_t u_y + \frac{c_s^2}{\rho_r}\partial_y \rho - \frac{\sigma}{2\,\rho_r}\left(-\partial_x \left(n_x n_y |\mathbf{C}|\right) + \partial_y \left(\left(1 - n_y^2\right)|\mathbf{C}|\right) - \partial_z \left(n_y n_z |\mathbf{C}|\right)\right) \\ \times \left(\frac{h_r c_r}{2\,s_\nu} - \frac{h_r c_r}{2\,s\prime_\nu}\right)\partial_{y,y} u_y + \left(\frac{h_r c_r}{4} + \frac{h_r c_r}{2\,s\prime_\nu}\right)\left(\partial_{x,x} u_y + \partial_{z,z} u_y\right) = \mathcal{O}(h^2).\end{aligned} \tag{A.28}$$

Collecting and adding order h^2 and h^3 of $EQ\,(3)$ yields the momentum equation in z-direction:

$$\begin{aligned}\partial_t u_z + \frac{c_s^2}{\rho_r}\partial_z \rho - \frac{\sigma}{2\,\rho_r}\left(-\partial_x \left(n_x n_z |\mathbf{C}|\right) - \partial_y \left(n_y n_z |\mathbf{C}|\right) + \partial_z \left(\left(1 - n_z^2\right)|\mathbf{C}|\right)\right) \\ \times \left(\frac{h_r c_r}{2\,s_\nu} - \frac{h_r c_r}{2\,s\prime_\nu}\right)\partial_{z,z} u_z + \left(\frac{h_r c_r}{4} + \frac{h_r c_r}{2\,s\prime_\nu}\right)\left(\partial_{x,x} u_z + \partial_{y,y} u_z\right) = \mathcal{O}(h^2).\end{aligned} \tag{A.29}$$

If we choose the relaxation rates and the hydrodynamic pressure as given by equations

$$\begin{aligned} s_\nu &= \frac{-2\,c_r\,h_r}{8\,\nu + c_r\,h_r}, \\ s\prime_\nu &= \frac{-2\,c_r\,h_r}{4\,\nu + c_r\,h_r}, \\ p &= c_s^2\,\rho, \end{aligned} \tag{A.30}$$

and we make use of the relation of the divergence form of the interfacial tension

$$\sigma\,\kappa\,n_\alpha\,\delta_\Gamma = \sigma\,\partial_\beta\left(\left(\delta_{\alpha\beta} - n_\alpha n_\beta\right)\delta_\Gamma\right) = \frac{\sigma}{2}\,\partial_\beta\left(\left(\delta_{\alpha\beta} - n_\alpha n_\beta\right)|\mathbf{C}|\right) \tag{A.31}$$

we obtain the following Stokes equations:

$$\partial_t u_\alpha + \frac{1}{\rho_r}\left(\partial_\alpha p - \sigma\,\kappa\,n_\alpha\,\delta_\Gamma\right) - \nu(\partial_{x,x} + \partial_{y,y} + \partial_{z,z})u_\alpha = \mathcal{O}(h^2), \quad \alpha = x, y, z. \tag{A.32}$$

The collision rates s_e and s_h are not relevant for the limit of the Stokes equations and can be chosen in the range]0, 2[to improve stability [86]. The optimal values for the MRT model depend on the specific system under consideration (geometry, initial and boundary conditions) and cannot be computed in advance. In the work of d'Humières and Ginzburg [37] favorable and general valid combinations of odd relaxation rates related to third order moments (s_h) and even relaxation rates related to second order moments (s_ν, $s\prime_\nu$) are given (two-relaxation-time model, TRT). These 'magic' collision numbers have been combined with advanced boundary condition schemes by Ginzburg et al. in [38,82] and allow to improve the accuracy of the scheme considerably. The D3Q13 Stokes model does not allow a TRT setup since we have different values for s_ν and $s\prime_\nu$. The collision rates are chosen as given by Eq. (17) and give good results for Stokes flow.

References

[1] R. Benzi, S. Succi, M. Vergassola, The lattice Boltzmann equation: theory and applications, Physics Reports 222 (3) (1992) 147–197.
[2] D.H. Rothman, S. Zaleski, Lattice-Gas Cellular Automata: Simple Models of Complex Hydrodynamics, Cambridge University Press, UK, 1997.

[3] S. Chen, G.D. Doolen, Lattice Boltzmann method for fluid flows, Annual Review of Fluid Mechanics 30 (1998) 329–364.
[4] S. Succi, The Lattice Boltzmann Equation for Fluid Dynamics and Beyond, Oxford University Press, 2001.
[5] D.H. Rothman, J.M. Keller, Immiscible cellular automaton fluids, Journal of Statistical Physics 52 (1988) 1119–1127.
[6] A.K. Gunstensen, D.H. Rothman, Lattice Boltzmann modell of immiscible fluids, Physical Review A 43 (8) (1991) 4320–4327.
[7] D. Grunau, S. Chen, K. Eggert, A lattice Boltzmann model for multiphase fluid flows, Physics of Fluids 5 (10) (1993) 2557–2562.
[8] X. Shan, H. Chen, Lattice Boltzmann model for simulating flows with multiple phases and components, Physical Review E 47 (1993) 1815–1819.
[9] M.R. Swift, W.R. Osborn, J.M. Yeomans, Lattice Boltzmann simulation of nonideal fluids, Physical Review Letters 75 (5) (1995) 830–833.
[10] I. Ginzburg, P.M. Adler, Surface tension models with different viscosities, Transport in Porous Media 20 (1995) 37–76.
[11] I. Ginzburg, Lattice Boltzmann modeling with discontinuous collision components: hydrodynamic and advection–diffusion equations, Journal of Statistical Physics 126 (2007) 157–206.
[12] U. D'Ortona, D. Salin, M. Cieplak, R.B. Rybka, J.R. Banavar, Two-color nonlinear Boltzmann cellular automata: surface tension and wetting, Physical Review E 51 (1995) 3718–3728.
[13] J. Tölke, M. Krafczyk, M. Schulz, E. Rank, Lattice Boltzmann Simulations of binary fluid flow through porous media, Philosophical Transactions of the Royal Society A-Mathematical, Physical and Engineering Sciences 360 (1792) (2002) 535–545.
[14] M. Latva-Kokko, D.H. Rothman, Diffusion properties of gradient-based lattice Boltzmann models of immiscible fluids, Physical Review E 71 (2005) 056702.
[15] I. Halliday, A.P. Hollis, C.M. Care, Lattice Boltzmann algorithm for continuum multicomponent flow, Physical Review E 76 (2007) 026708.
[16] T. Reis, P.J. Dellar, A volume-preserving sharpening approach for the propagation of sharp phase boundaries in multiphase lattice Boltzmann simulations, Computers & Fluids 46 (1) (2011) 417–421.
[17] X. He, S. Chen, R. Zhang, A lattice Boltzmann scheme for incompressible multiphase flow and its application in simulation of Rayleigh–Taylor instability, Journal of Computational Physics 152 (1999) 642–663.
[18] S.H. Kim, H. Pitsch, On the lattice Boltzmann method for fluid flow, Technical Report, Center for Turbulence Research, 2009, Annual Research Briefs 2009.
[19] P. Lallemand, L.S. Luo, Y. Peng, A lattice Boltzmann front-tracking method for interface dynamics with surface tension in two dimensions, Journal of Computational Physics 226 (2) (2007) 1367–1384.
[20] L.Q.E. Santos, P.C. Facin, P.C. Philippi, Lattice-Boltzmann model based on field mediators for immiscible fluids, Physical Review E 68 (2003) 056302.
[21] T.J. Spencer, I. Halliday, C.M. Care, A local Lattice Boltzmann method for multiple immiscible fluids and dense suspensions of drops, Philosophical Transactions of the Royal Society A-Mathematical, Physical and Engineering Sciences 369 (2011) 2255–2263.
[22] B. Ferréol, D.H. Rothman, Lattice-Boltzmann simulations of flow through Fontainebleau sandstone, Transport in Porous Media 20 (1995) 3–20.
[23] N. Martys, H. Chen, Simulation of multicomponent fluids in complex three-dimensional geometries by the lattice Boltzmann method, Physical Review E 53 (1996) 743–750.
[24] P.M. Adler, F.F. Thovert, Real porous media: local geometry and macroscopic properties, Applied Mechanics Reviews 51 (9) (1998) 537–585.
[25] S. Bekri, O. Vizikab, J.-F. Thovert, P.M. Adler, Binary two-phase flow with phase change in porous media, International Journal of Multiphase Flow 27 (2001) 477–526.
[26] S. Bekri, P.M. Adler, Dispersion in multiphase flow through porous media, International Journal of Multiphase Flow 28 (2002) 665–697.
[27] Z. Guo, T.S. Zhao, Lattice Boltzmann model for incompressible flows through porous media, Physical Review E 66 (2002) 036304.
[28] S. Bekri, J. Howard, J. Muller, P.M. Adler, Electrical resistivity index in multiphase flow through porous media, Transport in Porous Media 51 (1) (2003) 41–65.
[29] C. Pan, M. Hilpert, C.T. Miller, Lattice-Boltzmann simulation of two-phase flow in porous media, Water Resources Research 40 (2004).
[30] J. Tölke, S. Freudiger, M. Krafczyk, An adaptive scheme for LBE multiphase flow simulations on hierarchical grids, Computers & Fluids 35 (2006) 820–830.
[31] B. Ahrenholz, J. Tölke, P. Lehmann, A. Peters, A. Kaestner, M. Krafczyk, W. Durner, Prediction of capillary hysteresis in porous material using lattice Boltzmann methods and comparison to experimental data and a morphological pore network model, Advances in Water Resources 31 (2008) 1151–1173.
[32] Y.H. Qian, D. d'Humières, P. Lallemand, Lattice BGK models for Navier–Stokes equation, Europhysics Letters 17 (1992) 479–484.
[33] D. d'Humières, M. Bouzidi, P. Lallemand, Thirteen-velocity three-dimensional lattice Boltzmann model, Physical Review E 63 (2001) 066702.
[34] J. Tölke, TeraFLOP computing on a desktop PC with GPUs for 3D CFD, International Journal of Computational Fluid Dynamics 22 (7) (2008) 443–456.
[35] B. Lafaurie, C. Nardone, R. Scardovelli, S. Zaleski, G. Zanetti, Modelling merging and fragmentation in multiphase flows with surfer, Journal of Computational Physics 113 (1) (1994) 134–147.
[36] I. Ginzburg, Generic boundary conditions for lattice Boltzmann models and their application to advection and anisotropic dispersion equations, Advances in Water Resources 28 (2005) 1196–1216.
[37] D. d'Humières, I. Ginzburg, Viscosity independent numerical errors for lattice Boltzmann models: from recurrence equations to magic collision numbers, Computers and Mathematics with Applications 58 (5) (2009) 823–840.
[38] I. Ginzburg, F. Verhaeghe, D. d'Humières, Two-relaxation-time lattice Boltzmann scheme: about parametrization, velocity, pressure and mixed boundary conditions, Communications in Computational Physics 3 (2008) 427–478.
[39] H. Huang, D.T. Thorne, M.G. Schaap, M.C. Sukop, Proposed approximation for contact angles in Shan-and-Chen-type multicomponent multiphase lattice Boltzmann models, Physical Review E 76 (2007) 066701.
[40] S. Schmieschek, J. Harting, Contact angle determination in multicomponent lattice boltzmann simulations, Communications in Computational Physics 9 (2011) 1165–1178.
[41] A.J. Briant, P. Papatzacos, J.M. Yeomans, Lattice Boltzmann simulations of contact line motion in a liquid–gas system, Philosophical Transactions of the Royal Society A-Mathematical, Physical and Engineering Sciences 360 (2002) 485.
[42] A.J. Briant, A.J. Wagner, J.M. Yeomans, Lattice Boltzmann simulations of contact line motion. I. Liquid–gas systems, Physical Review E 69 (2004) 031602.
[43] J. Tölke, Gitter–Boltzmann–Verfahren zur Simulation von Zweiphasenströmunge, Ph.D. Thesis, TU München, 2001.
[44] M. Latva-Kokko, D.H. Rothman, Static contact angle in lattice Boltzmann models of immiscible fluids, Physical Review E 72 (2005) 046701.
[45] A.P. Hollis, T.J. Spencer, I. Halliday, C.M. Care, Dynamic wetting boundary condition for continuum hydrodynamics with muli-component lattice Boltzmann equation simulation method, IMA Journal of Applied Mathematics 76 (2011).
[46] S. Donath, Wetting models for a parallel high-performance free surface lattice Boltzmann method, Ph.D. Thesis, Technische Fakultät der Universität Erlangen-Nürnberg, 2011.
[47] P. Raiskinmäki, A. Shakib-Manesh, A. Jäsberg, A. Koponen, J. Merikoski, J. Timonen, Lattice-boltzmann simulation of capillary rise dynamics, Journal of Statistical Physics 107 (2002) 143–158. http://dx.doi.org/10.1023/A:1014506503793.
[48] M. Latva-Kokko, D.H. Rothman, Scaling of dynamic contact angles in a lattice-Boltzmann model, Physical Review Letters 98 (2007) 254503.
[49] D. Enskog, Inaugural Dissertation, Uppsala, 1917.
[50] S. Chapman, On the law of distribution of molecular velocities, and on the theory of viscosity and thermal conduction, in a non-uniform simple monatomic gas, Philosophical Transactions of the Royal Society A-Mathematical, Physical and Engineering Sciences 216 (1916) 279–348.
[51] S. Chapman, T.G. Cowling, The Mathematical Theory of Non-Uniform Gases, Cambridge University Press, 1990.
[52] S. Wolfram, Cellular automaton fluids: basic theory, Journal of Statistical Physics 45 (1986) 471–526.
[53] U. Frisch, D. d'Humières, B. Hasslacher, P. Lallemand, Y. Pomeau, J.-P. Rivet, Lattice gas hydrodynamics in two and three dimensions, Complex Systems 1 (1987) 75–136.
[54] T. Inamuro, M. Yoshino, F. Ogino, Accuracy of the lattice Boltzmann method for small Knudsen number with finite Reynolds number, Physics of Fluids 9 (1997) 3535.

[55] M. Junk, A. Klar, L.S. Luo, Asymptotic analysis of the lattice Boltzmann equation, Journal of Computational Physics 210 (2005) 676.
[56] L.S. Luo, Unified Theory of the lattice Boltzmann models for nonideal gases, Physical Review Letters 81 (8) (1998) 1618–1621.
[57] L.S. Luo, Theory of the lattice Boltzmann method: Lattice Boltzmann models for nonideal gases, Physical Review E 62 (2000) 4982–4996.
[58] L.S. Luo, S.S. Girimaji, Lattice Boltzmann model for binary mixtures, Physical Review E 66 (2002) 035301.
[59] L.S. Luo, S.S. Girimaji, Theory of the lattice Boltzmann method: two-fluid model for binary mixtures, Physical Review E 67 (2003) 036302.
[60] D. Kehrwald, Numerical analysis of Immiscible Lattice BGK, Ph.D. Thesis, Universität Kaiserslautern, 2003.
[61] R. Scardovelli, S. Zaleski, Direct numerical simulation of free-surface and interfacial flow, Annual Review of Fluid Mechanics 31 (1999) 567–603.
[62] M.M. Francois, S.J. Cummins, E.D. Dendy, D.B. Kothe, J.M. Sicilian, M.W. Williams, A balanced-force algorithm for continuous and sharp interfacial surface tension models within a volume tracking framework, Journal of Computational Physics 213 (1) (2006) 141–173.
[63] R.R. Nourgaliev, T.N. Dinh, B.R. Sehgal, On lattice Boltzmann modeling of phase transition in an isothermal non-ideal fluid, Nuclear Engineering and Design 213 (2002) 153–171.
[64] S.V. Lishchuk, C.M. Care, I. Halliday, Lattice Boltzmann algorithm for surface tension with greatly reduced microcurrents, Physical Review E 67 (2003) 036701.
[65] A. Cristea, V. Sofonea, Reduction of spurious velocity in finite difference lattice Boltzmann models for liquid–vapor systems, International Journal of Modern Physics C 14 (2003) 1251–1266.
[66] A.J. Wagner, The origin of spurious velocities in lattice Boltzmann, International Journal of Modern Physics B 17 (2003) 193–196.
[67] T. Lee, P.F. Fischer, Eliminating parasitic currents in the lattice Boltzmann equation method for nonideal gases, Physical Review E 74 (2006) 046709.
[68] C.M. Pooley, K. Furtado, Eliminating spurious velocities in the free-energy lattice Boltzmann method, Physical Review E 77 (2008) 046702.
[69] X. Shan, Analysis and reduction of the spurious current in a class of multiphase lattice Boltzmann models, Physical Review E 73 (2006) 047701.
[70] L. Wu, M. Tsutahara, L.S. Kim, M.Y. Ha, Three-dimensional lattice Boltzmann simulations of droplet formation in a cross-junction microchannel, International Journal of Multiphase Flow 34 (2008) 852–864.
[71] P.M. Dupuy, M. Fernandino, H.A. Jakobsen, H.F. Svendsen, Fractional step two-phase flow lattice Boltzmann model implementation, Journal of Statistical Mechanics: Theory and Experiment 6 (2009) P06014.
[72] D. Chiappini, G. Bella, S. Succi, F. Toschi, S. Ubertini, Improved lattice Boltzmann without parasitic currents for Rayleigh–Taylor instability, Communications in Computational Physics 7 (3) (2010) 423–444.
[73] D. Jamet, D. Torres, J.U. Brackbill, On the theory and computation of surface tension: the elimination of parasitic currents through energy conservation in the second-gradient method, Journal of Computational Physics 182 (1) (2002) 276.
[74] Y. Renardy, M. Renardy, Prost: a parabolic reconstruction of surface tension for the volume-of-fluid method, Journal of Computational Physics 183 (2) (2002) 400–421.
[75] I. Ginzburg, G. Wittum, Two-phase flows on interface refined grids modeled with vof, staggered finite volumes, and spline interpolants, Journal of Computational Physics 166 (2001).
[76] M. Herrmann, A balanced force refined level set grid method for two-phase flows on unstructured flow solver grids, Journal of Computational Physics 227 (2008).
[77] A.Q. Raeini, M.J. Blunt, B. Bijeljic, Modelling two-phase flow in porous media at the pore scale using the volume-of-fluid method, Journal of Computational Physics (2012).
[78] D.D. Joseph, M. Renardy, Y. Renardy, Instability of the flow of two immiscible liquids with different viscosities in a pipe, Journal of Fluid Mechanics 141 (1984) 309–317.
[79] L. Preziosi, K. Chen, D.D. Joseph, Lubricated pipelining: stability of core-annular flow, Journal of Fluid Mechanics 201 (1989) 323–356.
[80] H.H. Hu, D.D. Joseph, Lubricated pipelining: stability of core-annular flow. Part 2, Journal of Fluid Mechanics 205 (1989) 359–396.
[81] V.C. Kelessidis, A.E. Dukler, Modeling flow pattern transitions for upward gas–liquid flow in vertical concentric and eccentric annuli, International Journal of Multiphase Flow 15 (1989) 173–191.
[82] I. Ginzburg, F. Verhaeghe, D. d'Humières, Study of simple hydrodynamic solutions with the two-relaxation-times lattice Boltzmann scheme, Communications in Computational Physics 3 (2008) 519–581.
[83] A. Kuzmin, I. Ginzburg, A.A. Mohamad, The role of the kinetic parameter in the stability of two-relaxation-time advectiondiffusion lattice Boltzmann schemes, Computers and Mathematics with Applications 61 (12) (2011) 3417–3442.
[84] I. Ginzburg, D. d'Humières, A. Kuzmin, Optimal stability of advection–diffusion lattice boltzmann models with two relaxation times for positive/negative equilibrium, Journal of Statistical Physics 139 (2010) 1090–1143. http://dx.doi.org/10.1007/s10955-010-9969-9.
[85] H. Hammou, I. Ginzburg, M. Boulerhcha, Two-relaxation-times Lattice Boltzmann schemes for solute transport in unsaturated water flow, with a focus on stability, Advances in Water Resources 34 (6) (2011) 779–793.
[86] P. Lallemand, L.S. Luo, Theory of the lattice Boltzmann method: dispersion, dissipation, isotropy, Galilean invariance, and stability, Physical Review E 61 (6) (2000) 6546–6562.